A positioning algorithm for VLP in the presence of orientation uncertainty

Shiyin Li [a], Shengqiang Shen [a,b,*], Heidi Steendam [b]

[a] *School of Information and Control Engineering, China University of Mining and Technology, Xuzhou, China*
[b] *Telecommunications and Information Processing Department of Ghent University, Ghent, Belgium*

ARTICLE INFO

ABSTRACT

As the positioning accuracy of a visible light positioning (VLP) system is highly susceptible to changes in the orientation of the receiver, accurate knowledge of the receiver orientation is required. In practice, the orientation of the receiver is estimated with an external orientation estimation device. However, these devices generally suffer from drift and misalignment, causing an uncertainty in the measured orientation that will degrade the performance of standard positioning algorithms. In this paper, we derive a novel positioning algorithm that takes into account the effect of the orientation uncertainty. To this end, we need to cope with the non-linear relationship between the received signal strength (RSS) and the orientation uncertainty, which makes the likelihood function of the RSS, required to derive the maximum likelihood (ML) estimator, hard to obtain. To solve this issue, we consider the first and second-order Taylor series expansion of the RSS. Although the accuracy of the second-order approximation is better than the first-order approximation, the first-order approximation results in a closed-form expression for the likelihood function, while this is not possible with the second-order approximation. Because of this, we derive the ML estimator using the first-order approximation, and employ the multivariate gradient descent algorithm to obtain the position estimate. Computer simulations show that the proposed algorithm outperforms state-of-the-art VLP algorithms subject to orientation uncertainty.

© 2019 Elsevier B.V. All rights reserved.

1. Introduction

During the last decade, visible light positioning (VLP) received an increasing amount of attention. Compared to other indoor positioning approaches, it has several advantages [1]. Due to their long life-time and energy efficiency, visible light LEDs are gradually replacing traditional light sources for illumination. As VLP can coexist with lighting systems, this will reduce the installation cost. Further, VLP systems suffer less from interference as light is blocked by opaque walls. Finally, due to the directionality of the transmitter and the confine field-of-view (FOV) of the receiver, VLP systems are able to accurately estimate the receiver's position. These properties make VLP a promising alternative for indoor positioning, and several positioning algorithms have been proposed in the literature, e.g. [2–4].

Most VLP approaches extract the position from the received signal strength (RSS). However, the RSS not only depends on the position of the receiver, but also on its orientation. Most works on VLP restrict their attention to the case where the orientation of the receiver is parallel to the transmitter or the ceiling [5–10], and some recent works [11–14] consider the performance of the VLP system when the receiver is tilted. In [12], a method to compensate for the change of the RSS, caused by the tilted orientation, is proposed and the conclusion is that the tilting only results in a slight degradation of the performance, while [13,14] take advantage of angular diversity provided by the tilted orientation of the receiver to improve the performance. However, all these works assume the receiver's orientation is fixed and known, which is not realistic in practice. In practical situations, the orientation of the receiver is not fixed and perfectly known due to the following reasons. First, the receiver will be attached to a carrier or carried by a user, implying the orientation of the receiver may change during the movement of the receiver. Secondly, the external device to measure the orientation of the receiver will often be a Micro-Electro-Mechanical System (MEMS)-based inertial measurement unit (IMU), because of its low price and low power consumption, and the ease of integrating it on the receiver. However, MEMS-based inertial sensors experience severe biases and drift problems, leading to uncertainties in the orientation tracked by IMUs [15]. As a conclusion, the orientation is not perfectly known but is subject to noise. As this orientation
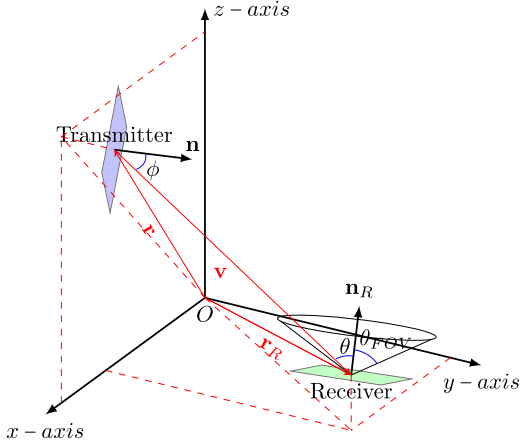
Fig. 1. System model.

uncertainty will affect the positioning performance of state-of-the-art algorithms, the uncertainty should be taken into account when designing a positioning algorithm. To the best of our knowledge, no other works considered the effect of orientation uncertainty on VLP performance.

In this paper, we propose a novel position estimation algorithm that takes into account the effect of the orientation uncertainty and that is based on the maximum likelihood (ML) principle. As the relationship between the RSS and the orientation of the receiver is highly non-linear, finding the likelihood function of the RSS, required to derive the ML estimator, is hard. To find a closed-form approximation for this likelihood function, we model the orientation uncertainty using concepts from the Lie algebra [16] and approximate the non-linear relationship between the RSS and orientation uncertainty using the Taylor series expansion of the RSS. The performance of the proposed estimator is compared to that of state-of-the-art estimators that are subject to orientation uncertainty, and the results show that the proposed algorithm outperforms the other algorithms. The paper is organized as follows. The system model and the orientation uncertainty model are presented in Section 2. The effect of the orientation uncertainty on the channel gain and the RSS are evaluated in Section 3. In this section, we also evaluate two approximations based on the Taylor series expansion of the RSS with as goal to simplify the likelihood function of the RSS. The novel positioning algorithm is discussed in Section 4 and in Section 5, we assess the performance of the proposed positioning algorithm.

2. System model

Let us consider a VLP system with multiple LEDs and a single receiver. To separate the signals from the different LEDs at the receiver, we assume a multiplexing protocol is used, e.g. frequency-division multiplexing (FDM) [17], time-division multiplexing (TDM) [18] or color-division multiplexing (CDM) [19]. In the remainder of this section, we will focus on the effect of the orientation uncertainty on the channel gain for a single LED and the photo diode (PD). In Section 4, we will discuss how the information from the different LEDs is combined to obtain the position estimate.

Following [20], the channel gain for the system shown in Fig. 1 can be modeled as

$$h = \frac{(\gamma + 1)A_R}{2\pi v^2} \cos^\gamma (\phi) \cos (\theta) \Pi \left(\frac{\theta}{\theta_{FOV}} \right), \tag{1}$$

where v is the distance between the LED and the receiver, ϕ the radiation angle at the LED, θ the incidence angle at the PD, A_R the

area of the PD, θ_{FOV} the field-of-view (FOV) of the PD, γ the Lambertian order of the LED, and $\Pi(\cdot)$ the rectangular function defined as

$$\Pi(x) \triangleq \begin{cases} 1, & |x| \leq 1, \\ 0, & |x| > 1. \end{cases} \tag{2}$$

The received signal strength yields

$$P = R_p P_t h + w, \tag{3}$$

where R_p is the responsivity of the PD, P_t the power transmitted by the LED and w is the shot noise, which is assumed to be zero-mean Gaussian distributed.

The LED has coordinates $\mathbf{r} \in \mathbb{R}^{3 \times 1}$ and normal $\mathbf{n} \in \mathbb{R}^{3 \times 1}$, i.e. the direction in which the LED is radiating, and the PD has coordinates $\mathbf{r}_R \in \mathbb{R}^{3 \times 1}$ and normal $\mathbf{n}_R \in \mathbb{R}^{3 \times 1}$, i.e. the direction in which the PD points. The orientation of the PD is expressed in terms of a rotation $\mathbf{R} \in SO(3)$[1] with respect to a reference orientation $\mathbf{n}_{R,0}$, i.e. $\mathbf{n}_R = \mathbf{R}\mathbf{n}_{R,0}$. As the reference orientation, we select the case of the receiver pointing straight upwards, i.e. where the normal of the receiver equals $\mathbf{n}_{R,0} = [0\ 0\ 1]^T$. The rotation matrix $\mathbf{R}$ is decomposed into a deterministic rotation $\tilde{\mathbf{R}} \in SO(3)$, corresponding to the known measurement or estimate of the orientation, and a random rotation $\mathbf{R}_\epsilon \in SO(3)$, containing the orientation uncertainty, with $\mathbf{R} = \mathbf{R}_\epsilon \cdot \tilde{\mathbf{R}}$. Using the concept of Lie groups, the random rotation can be expressed as

$$\mathbf{R}_\epsilon = \exp (\boldsymbol{\epsilon}_\times) \tag{4}$$

where $\boldsymbol{\epsilon} = [\epsilon_x\ \epsilon_y\ \epsilon_z]^T$ is a 3×1 random infinitesimal rotation vector and the operator $(\cdot)_\times$ converts the vector $\boldsymbol{\epsilon}$ into an element of the Lie algebra $\mathfrak{so}(3)$ of the 3D rotation group $SO(3)$:

$$\boldsymbol{\epsilon}_\times = \begin{bmatrix} 0 & -\epsilon_z & \epsilon_y \\ \epsilon_z & 0 & -\epsilon_x \\ -\epsilon_y & \epsilon_x & 0 \end{bmatrix} \in \mathfrak{so}(3). \tag{5}$$

We further define the receiver normal without orientation uncertainty as $\tilde{\mathbf{n}}_R = \tilde{\mathbf{R}}\mathbf{n}_{R,0}$.

The distribution of the rotation matrix $\mathbf{R}_\epsilon$ is determined by the distribution of the rotation vector $\boldsymbol{\epsilon}$. This rotation vector can be interpreted as an orientation error vector, which is a linear transformation of the Euler angles' error vector [21]. The Euler angles' error originate from small perturbations in the IMU device or the movement of the receiver, and can be modeled as statistically independent zero-mean random variables. Therefore, the rotation vector $\boldsymbol{\epsilon}$ will also be zero-mean Gaussian distributed.[2]

The channel gain depends on the orientation uncertainty through the incidence angle θ only. Let us define the incidence vector $\mathbf{v}$ as the vector between the LED and the PD, i.e. $\mathbf{v} = \mathbf{r}_R - \mathbf{r}$. Hence, the channel gain (1) can be rewritten as

$$h = K(\mathbf{n}, \mathbf{v}) \cos (\theta), \tag{6}$$

where $K(\mathbf{n}, \mathbf{v}) = \frac{(\gamma+1)A_R}{2\pi v^2} \cos^\gamma (\phi) \Pi (\theta/\theta_{FOV})$ is a function of $\mathbf{n}$ and $\mathbf{v}$, but independent of the orientation uncertainty $\boldsymbol{\epsilon}$ if the incidence angle is within the FOV. Further, using this definition, the incidence angle θ between $\mathbf{v}$ and the normal $\mathbf{n}_R$ of the receiver can be expressed as

$$\cos (\theta) = -\frac{\mathbf{n}_R^T \mathbf{v}}{\|\mathbf{v}\|} = -(\exp (\boldsymbol{\epsilon}_\times) \tilde{\mathbf{n}}_R)^T \bar{\mathbf{v}}, \tag{7}$$

where $\bar{\mathbf{v}} = \frac{\mathbf{v}}{\|\mathbf{v}\|}$. Similarly, the incidence angle $\tilde{\theta}$ between $\mathbf{v}$ and $\tilde{\mathbf{n}}_R$, i.e. without orientation uncertainty, equals $\cos (\tilde{\theta}) = -\tilde{\mathbf{n}}_R^T \bar{\mathbf{v}}$.

---

[1] $SO(3)$ represents the 3D rotation group.

[2] The assumption that the Euler angle error vector is zero-mean Gaussian distributed is confirmed in [22–24], where histograms of Euler angle errors were evaluated.

3. Approximation of the RSS

Let us consider a system where the receiver observes the light coming from N LEDs to determine its position $\mathbf{r}_R$. Given the observation vector $\mathbf{P} = [P_1, \ldots, P_N]^T$ of received signal strengths, the maximum likelihood (ML) estimator selects the vector $\hat{\mathbf{r}}_R$ that maximizes the likelihood function $p(\mathbf{P}; \mathbf{r}_R)$. However, the observation vector $\mathbf{P}$ not only depends on the position $\mathbf{r}_R$ of the receiver, but also on the orientation uncertainty $\boldsymbol{\epsilon}$, which should be considered as nuisance for the positioning problem. Hence, the likelihood function $p(\mathbf{P}; \mathbf{r}_R)$ must be obtained by marginalizing the joint likelihood function $p(\mathbf{P}, \boldsymbol{\epsilon}; \mathbf{r}_R) = p(\mathbf{P}|\boldsymbol{\epsilon}; \mathbf{r}_R) p(\boldsymbol{\epsilon}; \mathbf{r}_R)$ over $\boldsymbol{\epsilon}$. However, as the observation vector $\mathbf{P}$ depends on $\boldsymbol{\epsilon}$ in a non-linear way, a closed-form expression for $p(\mathbf{P}; \mathbf{r}_R)$ cannot be found. Although $p(\mathbf{P}; \mathbf{r}_R)$ could be obtained by Monte-Carlo simulations, the resulting procedure would be prohibitively complex for positioning purposes. To solve this issue, we will consider the Taylor series expansion of $\exp(\boldsymbol{\epsilon}_\times)$ to find an accurate approximation for the RSS that simplifies the derivation of the ML estimator, i.e.

$$\exp(\boldsymbol{\epsilon}_\times) = \mathbf{I}_{3\times3} + \boldsymbol{\epsilon}_\times + \frac{1}{2!}\boldsymbol{\epsilon}_\times^2 + \frac{1}{3!}\boldsymbol{\epsilon}_\times^3 + \cdots. \tag{8}$$

In the following, we restrict our attention to the case where the incidence angle $\theta \leq \theta_{FOV}$, i.e. where $\Pi(\theta/\theta_{FOV}) = 1$, as when $\theta > \theta_{FOV}$, $\Pi(\theta/\theta_{FOV}) = 0$.

3.1. First-order approximation

Discarding in (8) the second and higher order terms, the cosine of the incidence angle (7) can be approximated by

$$\cos(\theta) \approx -((\mathbf{I} + \boldsymbol{\epsilon}_\times)\tilde{\mathbf{n}}_R)^T\bar{\mathbf{v}}$$
$$= -\tilde{\mathbf{n}}_R^T\bar{\mathbf{v}} - (\tilde{\mathbf{n}}_R \times \bar{\mathbf{v}})^T\boldsymbol{\epsilon}, \tag{9}$$

where $\mathbf{a} \times \mathbf{b}$ is the cross product of the vectors $\mathbf{a}$ and $\mathbf{b}$. As a result, the channel gain (6) can be approximated by

$$h^{(1)} = -K(\mathbf{n}, \mathbf{v})\left(\tilde{\mathbf{n}}_R^T\bar{\mathbf{v}} + (\tilde{\mathbf{n}}_R \times \bar{\mathbf{v}})^T\boldsymbol{\epsilon}\right). \tag{10}$$

As the approximated channel gain (10) is a linear function of $\boldsymbol{\epsilon}$, the marginalization of $p(\mathbf{P}, \boldsymbol{\epsilon}; \mathbf{r}_R)$ is straightforward, i.e. $p(\mathbf{P}; \mathbf{r}_R)$ is Gaussian.

3.2. Second-order approximation

In this approximation for the channel gain, we also keep the quadratic terms in (8). Hence, the cosine of the incidence angle (7) can be approximated by

$$\cos(\theta) \approx -\left(\left(\mathbf{I} + \boldsymbol{\epsilon}_\times + \frac{1}{2}\boldsymbol{\epsilon}_\times^2\right)\tilde{\mathbf{n}}_R\right)^T\bar{\mathbf{v}}$$
$$= -\tilde{\mathbf{n}}_R^T\bar{\mathbf{v}} - (\tilde{\mathbf{n}}_R \times \bar{\mathbf{v}})^T\boldsymbol{\epsilon} - \frac{1}{4}\boldsymbol{\epsilon}^T\mathbf{A}\boldsymbol{\epsilon}, \tag{11}$$

where $\mathbf{A} = \bar{\mathbf{v}}_\times \tilde{\mathbf{n}}_{R\times} + \tilde{\mathbf{n}}_{R\times}\bar{\mathbf{v}}_\times$ is a 3×3 matrix that is constructed using the skew-symmetric matrices $\tilde{\mathbf{n}}_{R\times}$ and $\bar{\mathbf{v}}_\times$, defined in a similar way as (5). Denote $\boldsymbol{\Sigma}_{\boldsymbol{\epsilon}} = \mathbf{L}^T\mathbf{L}$ as the Cholesky decomposition of the covariance matrix $\boldsymbol{\Sigma}_{\boldsymbol{\epsilon}}$, where $\mathbf{L}$ is a lower triangular matrix, and $\mathbf{V}\boldsymbol{\Lambda}\mathbf{V}^T = \mathbf{L}\mathbf{A}\mathbf{L}^T$ as the eigenvalue decomposition of the matrix $\mathbf{L}\mathbf{A}\mathbf{L}^T$, where $\mathbf{V}$ is the orthonormal matrix whose columns are the eigenvectors of $\mathbf{L}\mathbf{A}\mathbf{L}^T$, and $\boldsymbol{\Lambda} = \text{diag}(\lambda_i)$ is a diagonal matrix whose elements λ_i are the eigenvalues of $\mathbf{L}\mathbf{A}\mathbf{L}^T$. Consequently, the channel gain (6) can be rewritten as

$$h^{(2)} = -K(\mathbf{n}, \mathbf{v})\left(\frac{1}{4}(\mathbf{x} + \mathbf{b})^T\boldsymbol{\Lambda}(\mathbf{x} + \mathbf{b}) - c\right), \tag{12}$$

with $\mathbf{x} = \mathbf{V}^T(\mathbf{L}^T)^{-1}\boldsymbol{\epsilon}$, $\mathbf{b} = 2\boldsymbol{\Lambda}^{-1}\mathbf{V}^T\mathbf{L}(\tilde{\mathbf{n}}_R \times \bar{\mathbf{v}})$ and $c = \frac{1}{4}\mathbf{b}^T\boldsymbol{\Lambda}\mathbf{b} - \tilde{\mathbf{n}}_R^T\bar{\mathbf{v}}$. As the components of the Gaussian distributed vector $\mathbf{x}$ are uncorrelated and have variance 1, the approximation (12) consists of

an indefinite quadratic form of standard normal random variables, because $\boldsymbol{\Lambda}$ contains both positive and negative eigenvalues. Hence, the channel gain (12) is distributed according to the weighted independent non-central chi-square distribution. Unfortunately, this distribution does not lead to a closed-form expression for the posterior pdf $p(\mathbf{P}; \mathbf{r}_R)$. Although in the literature some works are available that further approximate (12) to obtain a closed-form expression for the likelihood function [25–29], these works focus on positive semi-definite quadratic forms.

3.3. Evaluation of the approximations

In this section, we evaluate the accuracy of the two approximations discussed above through simulations. To this end, we consider the case where the position and the normal of the LED are given by $\mathbf{r} = [0, 0, 3]^T$ and $\mathbf{n} = [0, 0, -1]^T$, i.e. the LED points straight downwards. Further, the LED transmits a power $P_t = 1$ W and has Lambertian order $\gamma = 10$. For the receiver, we consider a photo diode with area $A_R = 1$ cm^2 and FOV $\theta_{FOV} = 85°$. The receiver is placed below the LED, i.e. $\mathbf{r}_R = [0, 0, 0]^T$, and two orientations are considered, i.e. $\tilde{\theta} = \pi/180$ and $\tilde{\theta} = \pi/6$. The covariance matrix $\boldsymbol{\Sigma}_{\boldsymbol{\epsilon}}$ of the orientation uncertainty is assumed to be $\boldsymbol{\Sigma}_{\boldsymbol{\epsilon}} = \sigma_{\boldsymbol{\epsilon}}^2\mathbf{I}_{3\times3}$, where $\sigma_{\boldsymbol{\epsilon}}^2 = 2.0 \times 10^{-2}$ rad^2.

We first simulated the effect of the orientation uncertainty on the channel gain h (1). The results for the two orientations $\tilde{\mathbf{n}}_R = [0, \sin(\pi/180), \cos(\pi/180)]^T$ and $\tilde{\mathbf{n}}_R = [0, \sin(\pi/6), \cos(\pi/6)]^T$ are shown in Fig. 2(a) and (b). As can be observed, when the tilt is small, i.e. for $\tilde{\mathbf{n}}_R = [0, \sin(\pi/180), \cos(\pi/180)]^T$, the histogram of the channel gain is asymmetrical, while for larger tilts, e.g. $\tilde{\mathbf{n}}_R = [0, \sin(\pi/6), \cos(\pi/6)]^T$, the distribution is more symmetrical. This can be explained graphically using Fig. 3. In this figure, we assume the orientation vector $\tilde{\mathbf{n}}_R$ is located in the $x - O - y$ plane, the vector $\bar{\mathbf{v}}$ (7) coincides with the y-axis, and the orientation uncertainty $\exp(\boldsymbol{\epsilon}_\times)$ rotates the orientation vector $\tilde{\mathbf{n}}_R$ in the $x - O - y$ plane, i.e. we restrict our attention to the 2D case for simplicity. As $\boldsymbol{\epsilon}$ is Gaussian distributed, the normal $\mathbf{n}_R$ has a circular-shaped Gaussian distribution with mean $\tilde{\mathbf{n}}_R$. Taking into account that $\cos(\theta) = -\mathbf{n}_R^T\bar{\mathbf{v}}$, the distribution of $\cos(\theta)$ corresponds to the projection of the circular-shaped Gaussian distribution of $\mathbf{n}_R$ on $\bar{\mathbf{v}}$. When $\tilde{\theta}$ is large, this projection will not alter the shape of the distribution drastically, so the distribution of $\cos(\theta)$ will still resemble a Gaussian distribution. However, when $\tilde{\theta}$ is small, the projection will result in an asymmetrical distribution for $\cos(\theta)$, making the distribution resemble more like a truncated chi-squared distribution. In our example, the channel gain h will not exceed $h_m = K(\mathbf{n}, \mathbf{v}) = 1.945 \times 10^{-5}$ W. This upper limit equals the maximum value of the channel gain, corresponding to the case where $\cos(\theta) = 1$, i.e. when $\theta = 0$. In Fig. 2, we also show the histograms for the first-order $h^{(1)}$ (10) and second-order $h^{(2)}$ (12) approximation. As can be observed, the distribution of the second-order approximation matches the distribution of the channel gain well, while the distribution of the first-order approximation may strongly deviate from the true distribution, especially when the incidence angle $\tilde{\theta}$ is small.

In Fig. 2, we illustrated that the distribution of the channel gain for the first-order approximation lacks accuracy especially when the incidence angle is small. In Fig. 4, we show the corresponding likelihood function. We assume the shot noise is zero-mean Gaussian distributed with variance $\sigma_w^2 = 1 \times 10^{-13}$ A^2. Although the distribution of the channel gain not always can be modelled as Gaussian, the likelihood function resembles Gaussian, even when the incidence angle is small. The likelihood function for the first-order approximation is also shown in Fig. 4. Because of the lack of accuracy of the first-order channel gain approximation, the deviation between the approximated likelihood function and the true likelihood function is larger for Case (a) corresponding to a small in-
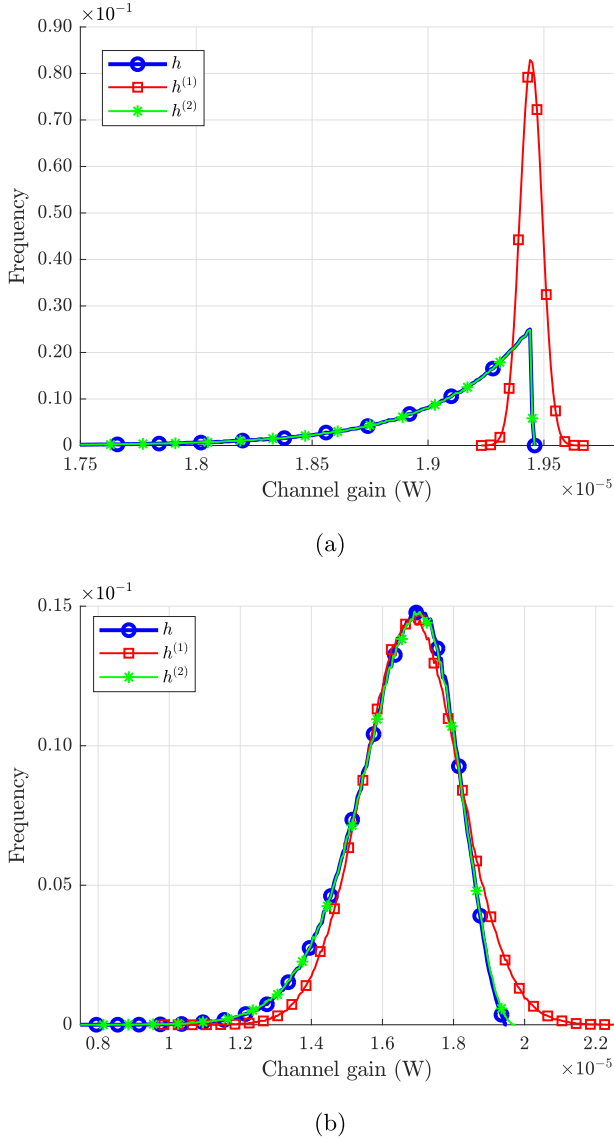
(a)

(b)

Fig. 2. Histogram of the channel gain for (a) $\tilde{\theta} = \pi/180$ and (b) $\tilde{\theta} = \pi/6$.
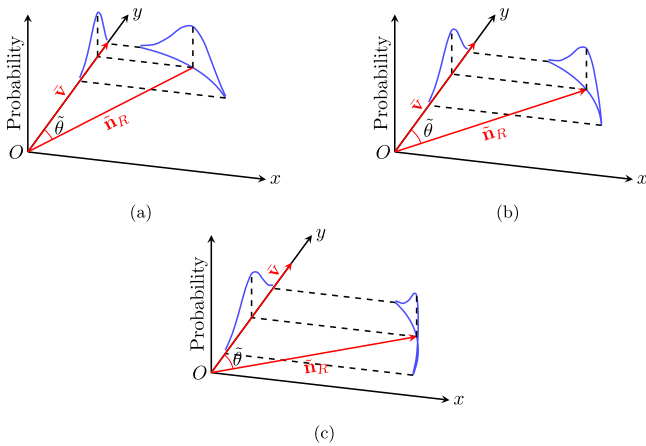

Fig. 3. Graphical explanation of the shape of the distribution of $\cos(\theta)$ for (a) $\tilde{\theta} = \pi/6$ (b) $\tilde{\theta} = \pi/4$ (c) $\tilde{\theta} = \pi/3$.
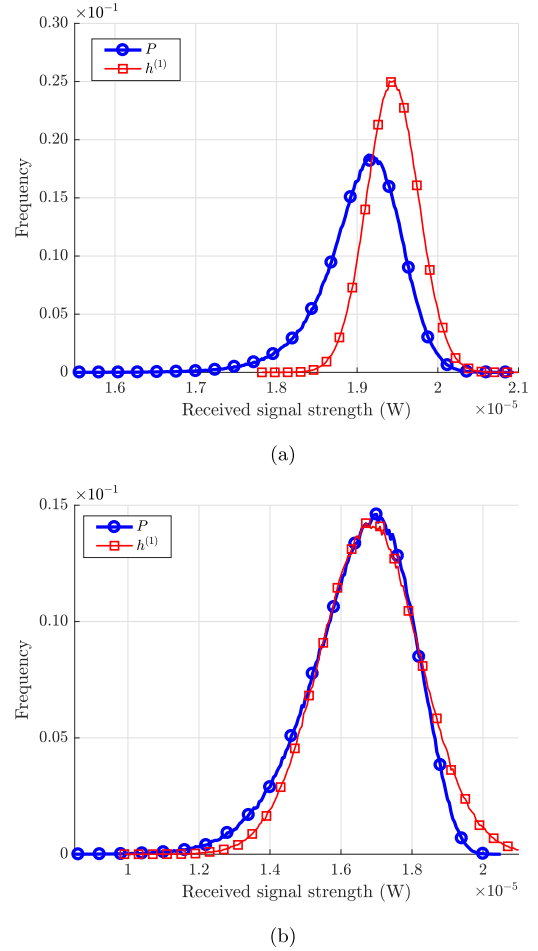

(a)

(b)

Fig. 4. Histogram of the received signal strength for (a) $\tilde{\theta} = \pi/180$ (b) $\tilde{\theta} = \pi/6$.

cidence angle than for Case (b). To estimate the position of the receiver, the ML estimator searches for the maximum of the likelihood function. Although the likelihood function deviates from its approximation, it can be observed that the position of the maxima of the two likelihood functions are close to each other. Hence, we expect that the first-order approximation will still result in an appropriate position estimate.

4. Improved RSS-based positioning

In the previous section, we evaluated two approximations for the channel gain in terms of accuracy and possibility to obtain a closed-form expression for the likelihood function. Taking into account that the first-order approximation results in a closed-form expression for the likelihood function, while this is not possible with the second-order approximation, we restrict our attention to the first-order approximation and derive a novel RSS-based positioning algorithm to cope with the orientation uncertainty. As stated in the previous section, we will consider the ML estimator of the position given the observation of the RSS values of N LEDs. We assume that all LEDs are of the same type and transmit the same power P_t. Employing the first-order approximation, the vector of observations yields

$$\mathbf{P} = \boldsymbol{\mu} + \mathbf{S}\boldsymbol{\epsilon} + \mathbf{w}, \tag{13}$$

where the ith component $[\boldsymbol{\mu}]_i$ of the vector $\boldsymbol{\mu}$ is the contribution of LED i defined as $-\breve{K}_i \tilde{\mathbf{n}}_R^T \bar{\mathbf{v}}_i$, with $\breve{K}_i = R_p P_t K(\mathbf{n}_i, \mathbf{v}_i)$. Further, $\mathbf{S} \in \mathbb{R}^{N \times 3}$ is the matrix having as i-th row $[\mathbf{S}]_i = -\breve{K}_i (\tilde{\mathbf{n}}_R \times \bar{\mathbf{v}})^T$, i.e. the contribution from LED i (see (10)). Taking into account that
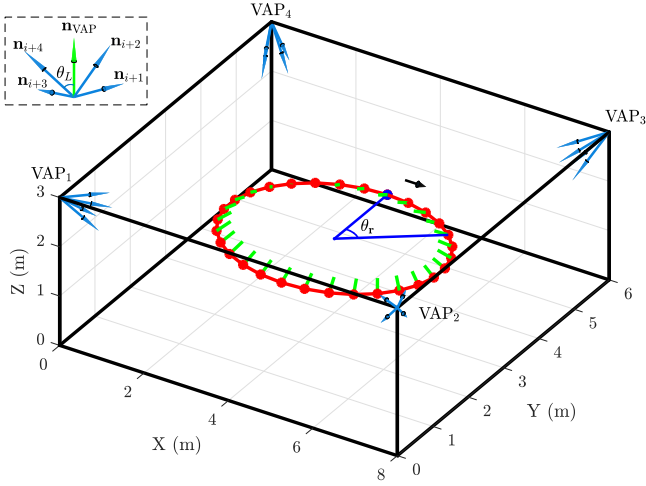
Fig. 5. Simulation setup, the receiver follows an elliptical path (red dotted curve) and has orientation indicated by the green lines. (For interpretation of the references to colour in this figure legend, the reader is referred to the web version of this article.)

both $\boldsymbol{\epsilon}$ and $\mathbf{w}$ are zero-mean Gaussian distributed, the likelihood function $p(\mathbf{P}; \mathbf{r}_R)$ is Gaussian distributed with average $\boldsymbol{\mu}$ and covariance matrix $\boldsymbol{\Sigma_P}$:

$$p(\mathbf{P}; \mathbf{r}_R) = \det(2\pi\,\boldsymbol{\Sigma_P})^{-\frac{1}{2}} \exp\left(-\frac{1}{2}\|\mathbf{P}-\boldsymbol{\mu}\|_{\boldsymbol{\Sigma_P}}^2\right), \tag{14}$$

where $\det(\cdot)$ denotes the determinant of a matrix, $\|\cdot\|_{\boldsymbol{\Sigma}}^2$ is the squared Mahalanobis' distance with respect to covariance matrix $\boldsymbol{\Sigma}$, i.e. $\|\mathbf{x}\|_{\boldsymbol{\Sigma}}^2 = \mathbf{x}^T\boldsymbol{\Sigma}^{-1}\mathbf{x}$ and $\boldsymbol{\Sigma_P} = \boldsymbol{\Sigma_S} + \sigma_w^2\mathbf{I}_N$ with $\boldsymbol{\Sigma_S} = \mathbf{S}\boldsymbol{\Sigma_{\epsilon}}\mathbf{S}^T$.

The ML estimate of $\mathbf{r}_R$ is defined as

$$\hat{\mathbf{r}}_R = \arg\max_{\mathbf{r}_R} \mathcal{L}(\mathbf{P}; \mathbf{r}_R), \tag{15}$$

where the log-likelihood function $\mathcal{L}(\mathbf{P}; \mathbf{r}_R)$ is given by

$$\mathcal{L}(\mathbf{P}; \mathbf{r}_R) = \text{const} - \frac{1}{2}\ln\det(\boldsymbol{\Sigma_P}) - \frac{1}{2}\|\mathbf{P}-\boldsymbol{\mu}\|_{\boldsymbol{\Sigma_P}}^2. \tag{16}$$

As the covariance matrix $\boldsymbol{\Sigma_P}$ depends on $\mathbf{r}_R$ through the matrix $\mathbf{S}$, a closed-form expression for the ML estimate (15) is generally not available. Hence, we consider the multivariate gradient descent algorithm to solve the optimization problem:

$$\mathbf{r}_R^{t+1} = \mathbf{r}_R^t - \eta\{\nabla\mathcal{L}(\mathbf{P}; \mathbf{r}_R^t)\} \tag{17}$$

where η is the step size, and the gradient $\nabla\mathcal{L}(\mathbf{P}; \mathbf{r}_R)$ is defined as

$$\nabla\mathcal{L}(\mathbf{P}; \mathbf{r}_R) = \left[\frac{\partial\mathcal{L}(\mathbf{P}; \mathbf{r}_R)}{\partial r_x} \quad \frac{\partial\mathcal{L}(\mathbf{P}; \mathbf{r}_R)}{\partial r_y} \quad \frac{\partial\mathcal{L}(\mathbf{P}; \mathbf{r}_R)}{\partial r_z}\right]^T, \tag{18}$$

with (19), (20), and

$$\frac{\partial\mathcal{L}(\mathbf{P}; \mathbf{r}_R)}{\partial r_l} = -\frac{1}{2}\text{tr}\left(\boldsymbol{\Sigma_P}^{-1}\left\{\frac{\partial\boldsymbol{\Sigma_P}}{\partial r_l}\right\}\right)$$
$$-\frac{1}{2}\text{tr}\left(-\boldsymbol{\Sigma_P}^{-1}\left\{\frac{\partial\boldsymbol{\Sigma_P}}{\partial r_l}\right\}\boldsymbol{\Sigma_P}^{-1}(\mathbf{P}-\boldsymbol{\mu})(\mathbf{P}-\boldsymbol{\mu})^T\right.$$
$$\left.-2\boldsymbol{\Sigma_P}^{-1}(\mathbf{P}-\boldsymbol{\mu})\left\{\frac{\partial\boldsymbol{\mu}}{\partial r_l}\right\}^T\right), \tag{19}$$

$$\left[\frac{\partial\boldsymbol{\Sigma_P}}{\partial r_l}\right]_{i,j} = [\boldsymbol{\Sigma_S}]_{i,j}\left[\left(\frac{\gamma\mathbf{n}_i}{\mathbf{n}_i^T\mathbf{v}_i} + \frac{\gamma\mathbf{n}_j}{\mathbf{n}_j^T\mathbf{v}_j}\right) - \left(\frac{(\gamma+3)\mathbf{v}_i}{\|\mathbf{v}_i\|^2} + \frac{(\gamma+3)\mathbf{v}_j}{\|\mathbf{v}_j\|^2}\right)\right]_l$$
$$+ \frac{\check{K}_i}{\|\mathbf{v}_i\|}\frac{\check{K}_j}{\|\mathbf{v}_j\|}\left[\tilde{\mathbf{n}}_R \times \left(\boldsymbol{\Sigma_{\epsilon}}\left((\mathbf{v}_i+\mathbf{v}_j) \times \tilde{\mathbf{n}}_R\right)\right)\right]_l, \tag{20}$$

$$\left[\frac{\partial\boldsymbol{\mu}}{\partial r_l}\right]_i = \left[[\boldsymbol{\mu}]_i\left(\frac{\gamma\mathbf{n}_i}{\mathbf{n}_i^T\mathbf{v}_i} - \frac{(\gamma+3)\mathbf{v}_i}{\|\mathbf{v}_i\|^2}\right) - \frac{\check{K}_i\tilde{\mathbf{n}}_R}{\|\mathbf{v}_i\|}\right]_l, \tag{21}$$

and $\text{tr}(\cdot)$ denotes the trace of a matrix.

5. Numerical results

In this section, we evaluate the performance of the proposed estimator through computer simulations. In our simulations, we consider an 8 m × 6 m × 3 m area with four visible light access points (VAPs) mounted in the upper corners of the area, as shown in Fig. 5 [30]. Each VAP is equipped with four LEDs and is tilted towards the center of the area, with the angle between the normal of the VAP and the ceiling equal to $\theta_{\text{VAP}} = \pi/6$. As shown in Fig. 5, the four LEDs of the VAP are placed symmetrically around the center of the VAP, and are tilted away from the center of the VAP, i.e. the angle between the normal of the VAP and the normal of a LED is $\theta_L = \pi/9$. Hence, the normal vector of the kth VAP, $k \in \{1, 2, 3, 4\}$ equals $\mathbf{n}_k = [\frac{\sqrt{2}}{2}\cos(k\pi/2), \frac{\sqrt{2}}{2}\sin(k\pi/2), -\frac{1}{2}]^T$, and the normal of the mth LED of the kth VAP, $m \in \{1, 2, 3, 4\}$ is given by $\mathbf{n}_{k,m} = \mathbf{R}(\theta_L, \mathbf{z}_m)\mathbf{n}_k$, where $\mathbf{R}(\theta_L, \mathbf{z}_m)$ denotes the Rodrigues' rotation formula [31] that computes the rotation matrix in $SO(3)$ from $\mathbf{z}_m = [\cos(m\pi/2), \sin(m\pi/2), 0]^T$ and θ_L. All LEDs have a transmit power of 1 W and a Lambertian order $\gamma = 10$. The receiver has a FOV of $\theta_{FOV} = 85°$ and an area of $A_R = 1$ cm^2. We assume the receiver is subject to an orientation uncertainty with covariance matrix $\boldsymbol{\Sigma_{\epsilon}} = \sigma_{\epsilon}^2\mathbf{I}_{3\times3}$. This variance is taken within the interval $\sigma_{\epsilon}^2 \in [0.1 \times 10^{-2}, 2.0 \times 10^{-2}]$ rad^2.[3] Finally, the shot noise variance is set to $\sigma_w^2 = 1 \times 10^{-13}$ A^2 [30].

To evaluate the performance of the proposed estimator (RSS-P), we consider an elliptical path for the receiver that is located in a plane parallel to the ceiling. The ellipse has a semi-major axis of 2 m and a semi-minor axis of 1.5 m, and the coordinates of the center of the ellipse are $[4.0, 3.0, 1.5]^T$ m. The path of the receiver starts at the coordinates $[4.0, 4.5, 1.5]^T$ m (the blue dot) and follows the ellipse clockwise. We consider two cases. In Case 1, $\tilde{\mathbf{n}}_R$ points straight upwards, i.e. the noise-free rotation equals $\tilde{\mathbf{R}} = \mathbf{I}_{3\times3}$. In Case 2, $\tilde{\mathbf{n}}_R$ is tilted towards the center of the area over an angle of $2\pi/9$ with respect to the tangent of the path at the current position (the normals of receiver in this case are shown by the green lines at each position). We compute the root mean squared error (RMSE) of the position estimate along this path for the proposed estimator and two other estimators, i.e. the weighted AOA method and the RSS-based method (RSS-Ş) both presented in [30]. The weighted AOA method estimates the position from the AOA between the receiver and each VAP, weighted with the corresponding RSS. In this method, the AOA with respect to a VAP is approximated by the orientation of the LED that gives the largest RSS within this VAP. Hence, this method gives only a rough estimate for the AOA. On the other hand, in the RSS-Ş method, the position is extracted from the RSS information using the ML estimation, similarly as in the proposed estimation (RSS-P). However, in contrast to the proposed method, the RSS-Ş estimation does not take into account the orientation uncertainty. Both the RSS-Ş method and the proposed method are iterative methods that need proper initialization to converge. To initialize these iterative methods, the rough estimates attained with the weighted AOA estimation are used. The RMSE of the three methods are shown in Fig. 6, along with the root of the Cramér-Rao bound (rCRB) from [30], which assumes no orientation uncertainty is present (rCRB-nOU). As can be observed, the weighted AOA method (AOA) performs
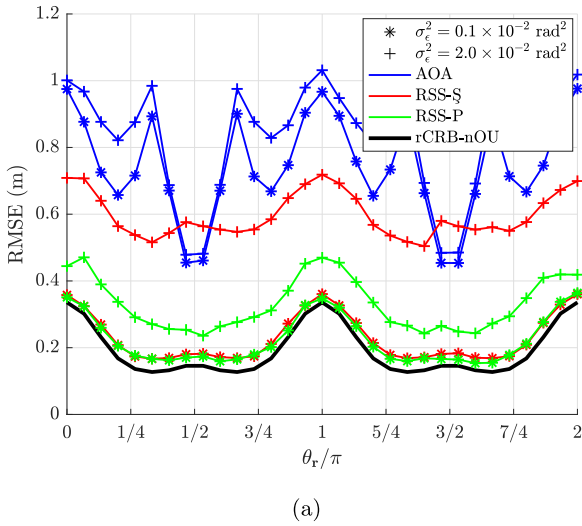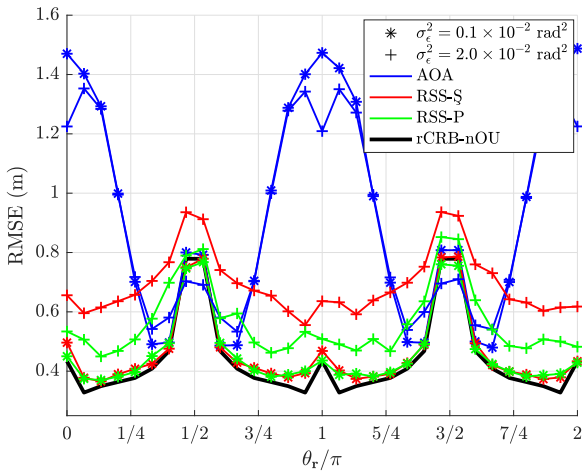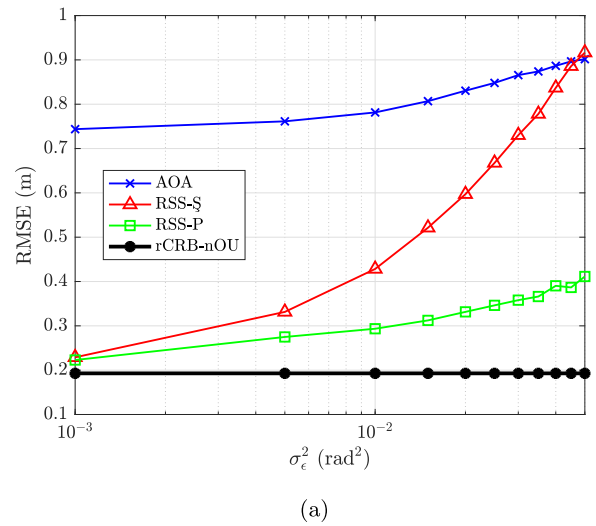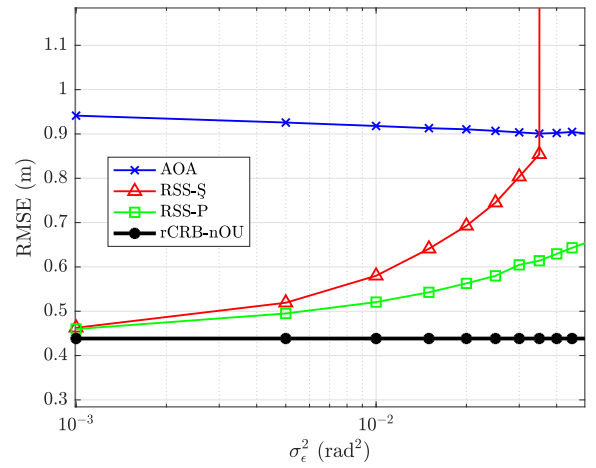

Fig. 6. Performance of estimators for (a) Case 1 (b) Case 2.

Fig. 7. RMSE versus σ_ϵ^2 for (a) Case 1 (b) Case 2.

worst, and its RMSE strongly fluctuates along the considered path, while the RMSE of the RSS-based methods fluctuate less. Comparing the RMSE performance of the RSS-based methods for the two cases, we observe that the RMSE is on the average lower in Case 1 than in Case 2, and we notice that the RMSE behaves differently for the two cases, In Case 1 (Fig. 6a), where the receiver points straight upwards, the highest RMSE is found when the receiver is near the semi-minor axis ($\theta_r = k\pi, k = 0, 1, 2$), and the lowest RMSE when it is near the semi-major axis ($\theta_r = \pi/2 + k\pi, k = 0, 1$). This can be explained as follows. When near the semi-minor axis, the receiver is closer to the center of the area. Because the receiver points straight upwards, the incidence angle for the nearest VAPs will be larger than for the case where the receiver is near the semi-major axis. Hence, for the nearest VAPs, the RSS will be lower. As the positioning performance is mainly determined by the strongest RSS contributions, this implies the RMSE performance will degrade when this strongest RSS contribution reduces. On the other hand, in Case 2 (Fig. 6b), when the receiver is tilted towards the center of the area, the highest RMSE is found when the receiver is near the semi-major axis ($\theta_r = \pi/2 + k\pi, k = 0, 1$). In this case, as the receiver is tilted towards the center of the area, it is tilted away from the nearest VAPs. Hence, incidence angle for the light coming from the nearest VAPs strongly increases, resulting in lower RSS values. Near the semi-minor axis, the relative increase in the inci-

dence angle for the nearest VAPs will be smaller as the receiver is further away from the nearest VAPs, implying the effect of the tilt on the RSS values is smaller. Hence, while in Case 1, the reduction of the RSS for the nearest VAPs, and thus the performance reduction, is mainly due to the distance of the receiver to the nearest VAPs, in Case 2, the reduction of the RSS for the nearest VAPs is due to the tilt, and the largest reduction of the RSS occurs for different receiver position than in Case 1. As in Case 2 the receiver is tilted away from the nearest VAPs, it will receive less light from the nearest VAPs, implying the RMSE performance for Case 2 will be on the average worse than that for Case 1. In both cases, the best performance is obtained with the proposed method and the resulting RMSE is close to the rCRB-nOU, indicating the proposed estimator performs close to optimal.

In Fig. 7, we show the average RMSE over the entire path as function of the variance σ_ϵ^2. As can be observed in the figure, although the weighted AOA method performs worse for small σ_ϵ^2, it is largely insensitive to the orientation uncertainty, while both RSS-based methods have a degrading performance for increasing σ_ϵ^2 compared with the CRB in the absence of orientation uncertainty. The degradation of the proposed method is smaller than that of the RSS-Ş method, which could be expected as the RSS-Ş method does not take into account the orientation uncertainty. Further, it can be observed that, when σ_ϵ^2 is large, the RMSE of
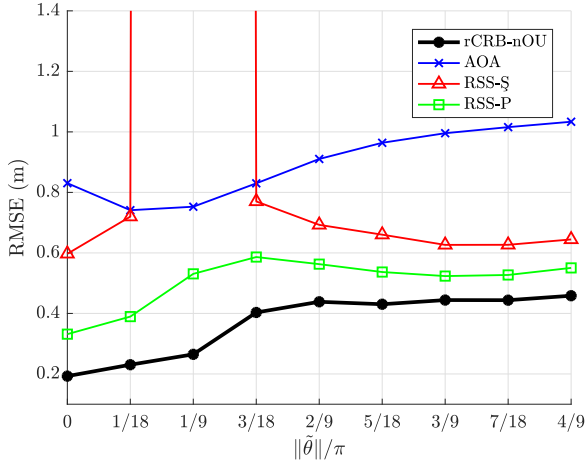
Fig. 8. RMSE versus $\|\tilde{\theta}\|$ for $\sigma_\epsilon^2 = 2.0 \times 10^{-2}$.

(a)

(b)

Fig. 9. RMSE versus $N = 4 + M^2$ VAPs for (a) Case 1 (b) Case 2.

the RSS-Ş estimator becomes worse than that of the weighted AOA method in Case 1, while for Case 2, the RSS-Ş estimator is even not able to return a proper estimate of position.

Until now, we limited our investigations to the evaluation of the performance of the estimators for two tilt angles $\tilde{\theta}$ of the receiver along the elliptical path only, i.e. $\tilde{\theta} = 0$ and $\tilde{\theta} = 2\pi/9$. Now, we will investigate the effect of the tilt angle $\tilde{\theta}$ on the performance. Fig. 8 gives the average RMSE over the entire path as function of the tilt angle $\tilde{\theta}$ for $\sigma_\epsilon^2 = 2.0 \times 10^{-2}$ rad². As expected, the best performance is obtained with the proposed method, and its RMSE is close to the rCRB-nOU. It can also be observed that the RSS-Ş method in general performs better than the weighted AOA method, but near the tilt angle $\|\tilde{\theta}\| = \pi/9$, the iterative procedure used in the RSS-Ş method fails to converge.

In this part, we evaluate the effect of the number of LEDs on the performance of the estimators. We consider the simulation setup shown in Fig. 5, but with M^2 extra VAPs mounted on the ceiling, i.e. the total number of VAPs now equals $N = 4 + M^2$. These extra VAPs are evenly distributed over the area, i.e. defining the length of the area $X = 8$ m and the width $Y = 6$ m, the position of the VAPs are $[i\frac{X}{M+1}, j\frac{Y}{M+1}]^T$, with $i, j \in \{1, \ldots, M\}$ and point straight down, i.e. $\theta_{VAP} = \pi/2$. Fig. 9 illustrates the average RMSE over the entire path as a function of the number of VAPs for $\sigma_\epsilon^2 = 2.0 \times 10^{-2}$ rad². It can be observed that this result is consistent with our previous results, i.e. the proposed method achieves the best performance and its RMSE is close to the rCRB-nOU. Further, as expected, Fig. 9 shows that when N increases all estimators trend to have a better performance.

6. Conclusion

In this paper, we design a novel RSS-based positioning method for VLP in the presence of orientation uncertainty. This orientation uncertainty, which is modeled using the concept of Lie algebra, is included in the expression of the received signal strength. To be able to apply maximum likelihood estimation of receiver's position, we need a closed-form expression for the likelihood function of the RSS. Because the relationship between the RSS and the orientation uncertainty is non-linear, finding an exact closed-form expression is not possible. Therefore, we consider two Taylor expansion based approximations to find a closed-form expression for the likelihood function. We show that although the second-order approximation closely matches the true distribution, it will not lead to a closed-form expression for the likelihood function, while the first-order approximation results in a simple closed-form expression at the expense of some accuracy loss. The resulting likelihood
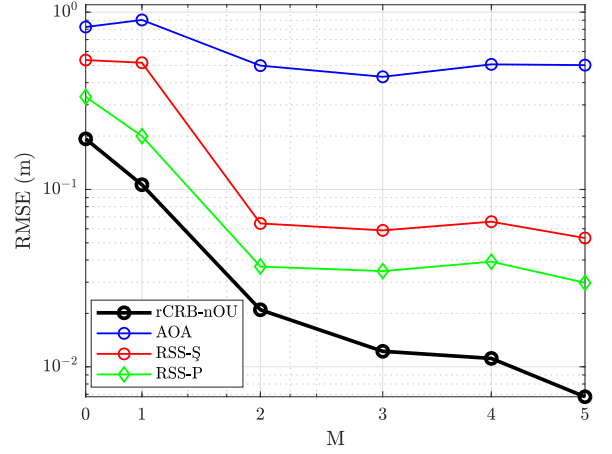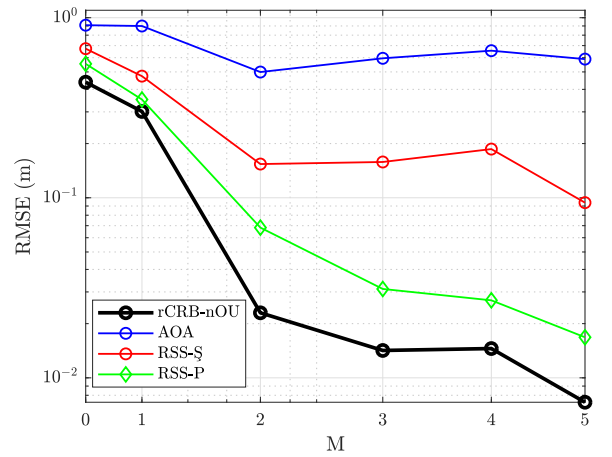
function is optimized using an iterative procedure based on gradient descent algorithm in order to find the position estimate. We compare the performance of the proposed estimator with state-of-the-art estimators and show that in the presence of orientation uncertainty, the proposed estimator outperforms the state-of-the-art estimators. In this paper, we restricted our attention to the effect of orientation uncertainty on RSS-based VLP. However, also in time-of-arrival (TOA)-based VLP [36] and time-difference-of-arrival (TDOA)-based VLP [37], the attenuation factor of the optical channel depends on the cosine of the incidence angle (7). Hence, their performance will also be affected by the orientation uncertainty. We expected that the first-order approximation will also be suitable for these systems to simplify the model and to derive algorithms to counteract the effects of the orientation uncertainty.

Conflicts of interest

The authors declare that they have no known competing financial interests or personal relationships that could have appeared to influence the work reported in this paper.

Acknowledgments

References

[1] N.U. Hassan, A. Naeem, M.A. Pasha, T. Jadoon, C. Yuen, Indoor positioning using visible LED lights: a survey, ACM Comput. Surv. 48 (2) (2015) 20:1–20:32, doi:10.1145/2835376.

[2] D. Wu, W.D. Zhong, Z. Ghassemlooy, C. Chen, Short-range visible light ranging and detecting system using illumination light emitting diodes, IET Optoelectron. 10 (3) (2016) 94–99, doi:10.1049/iet-opt.2015.0066.

[3] H. Steendam, A 3-D positioning algorithm for AOA-based VLP with an aperture-based receiver, IEEE J. Sel. Areas Commun. 36 (1) (2018) 23–33, doi:10.1109/JSAC.2017.2774478.

[4] Y. Hou, S. Xiao, M. Bi, Y. Xue, W. Pan, W. Hu, Single LED beacon-based 3-D indoor positioning using off-the-shelf devices, IEEE Photonics J. 8 (6) (2016) 1–11, doi:10.1109/JPHOT.2016.2636021.

[5] S.H. Yang, E.M. Jeong, D.R. Kim, H.S. Kim, Y.H. Son, S.K. Han, Indoor three-dimensional location estimation based on LED visible light communication, Electron. Lett. 49 (1) (2013) 54–56, doi:10.1049/el.2012.3167.

[6] H.S. Kim, D.R. Kim, S.H. Yang, Y.H. Son, S.K. Han, An indoor visible light communication positioning system using a RF carrier allocation technique, J. Lightwave Technol. 31 (1) (2013) 134–144, doi:10.1109/JLT.2012.2225826.

[7] S.-Y. Jung, S.R. Lee, C.-S. Park, Indoor location awareness based on received signal strength ratio and time division multiplexing using light-emitting diode light, Opt. Eng. 53 (1) (2014) 016106.

[8] N.A. Mohammed, M.A. Elkarim, Exploring the effect of diffuse reflection on indoor localization systems based on RSSI-VLC, Opt. Express 23 (16) (2015) 20297–20313, doi:10.1364/OE.23.020297.

[9] H. Huang, L. Feng, P. Guo, A. Yang, G. Ni, Iterative positioning algorithm to reduce the impact of diffuse reflection on an indoor visible light positioning system, Opt. Eng. 55 (6) (2016) 066117.

[10] S. Shawky, M.A. El-Shimy, Z.A. El-Sahn, M.R.M. Rizk, M.H. Aly, Improved VLC-based indoor positioning system using a regression approach with conventional RSS techniques, in: 2017 13th International Wireless Communications and Mobile Computing Conference (IWCMC), 2017, pp. 904–909, doi:10.1109/IWCMC.2017.7986406.

[11] H. Steendam, T.Q. Wang, J. Armstrong, Theoretical lower bound for indoor visible light positioning using received signal strength measurements and an aperture-based receiver, J. Lightwave Technol. 35 (2) (2017) 309–319, doi:10.1109/JLT.2016.2645603.

[12] E.M. Jeong, S.H. Yang, H.S. Kim, S.K. Han, Tilted receiver angle error compensated indoor positioning system based on visible light communication, Electron. Lett. 49 (14) (2013) 890–892, doi:10.1049/el.2013.1368.

[13] S.H. Yang, H.S. Kim, Y.H. Son, S.K. Han, Three-dimensional visible light indoor localization using AOA and RSS with multiple optical receivers, J. Lightwave Technol. 32 (14) (2014) 2480–2485, doi:10.1109/JLT.2014.2327623.

[14] Q.-L. Li, J.-Y. Wang, T. Huang, Y. Wang, Three-dimensional indoor visible light positioning system with a single transmitter and a single tilted receiver, Opt. Eng. 55 (10) (2016) 106103, doi:10.1117/1.OE.55.10.106103.

[15] G. Pons-Moll, A. Baak, J. Gall, L. Leal-Taixé, M. Müller, H.P. Seidel, B. Rosenhahn, Outdoor human motion capture using inverse kinematics and von Mises-Fisher sampling, in: 2011 International Conference on Computer Vision, 2011, pp. 1243–1250, doi:10.1109/ICCV.2011.6126375.

[16] T.D. Barfoot, P.T. Furgale, Associating uncertainty with three-dimensional poses for use in estimation problems, IEEE Trans. Rob. 30 (3) (2014) 679–693, doi:10.1109/TRO.2014.2298059.

[17] U. Nadeem, N.U. Hassan, M.A. Pasha, C. Yuen, Indoor positioning system designs using visible LED lights: performance comparison of TDM and FDM protocols, Electron. Lett. 51 (1) (2015) 72–74, doi:10.1049/el.2014.1668.

[18] M. Biagi, A.M. Vegni, T.D.C. Little, LAT indoor MIMO-VLC –Localize, access and transmit, in: 2012 International Workshop on Optical Wireless Communications (IWOW), 2012, pp. 1–3, doi:10.1109/IWOW.2012.6349698.

[19] S. Pergoloni, Z. Mohamadi, A.M. Vegni, Z. Ghassemlooy, M. Biagi, Metameric indoor localization schemes using visible lights, J. Lightwave Technol. 35 (14) (2017) 2933–2942, doi:10.1109/JLT.2017.2706527.

[20] J.M. Kahn, J.R. Barry, Wireless infrared communications, Proc. IEEE 85 (2) (1997) 265–298, doi:10.1109/5.554222.

[21] M.D. Shuster, A survey of attitude representations, Navigation 8 (9) (1993) 439–517.

[22] M. Zhang, J.D. Hol, L. Slot, H. Luinge, Second order nonlinear uncertainty modeling in strapdown integration using MEMS IMUs, in: 14th International Conference on Information Fusion, 2011, pp. 1–7.

[23] A. Jiménez, F. Seco, F. Zampella, J. Prieto, J. Guevara, Improved heuristic drift elimination with magnetically-aided dominant directions (MiHDE) for pedestrian navigation in complex buildings, J. Locat. Based Serv. 6 (3) (2012) 186–210, doi:10.1080/17489725.2012.687779.

[24] F.J. Wouda, M. Giuberti, G. Bellusci, P.H. Veltink, Estimation of full-body poses using only five inertial sensors: an eager or lazy learning approach? Sensors 16 (12) (2016) 2138.

[25] D.A. Bodenham, N.M. Adams, A comparison of efficient approximations for a weighted sum of chi-squared random variables, Stat. Comput. 26 (4) (2016) 917–928, doi:10.1007/s11222-015-9583-4.

[26] H. Liu, Y. Tang, H.H. Zhang, A new chi-square approximation to the distribution of non-negative definite quadratic forms in non-central normal variables, Comput. Stat. Data Anal. 53 (4) (2009) 853–856, doi:10.1016/j.csda.2008.11.025.

[27] A. Castaño-Martínez, F. López-Blázquez, Distribution of a sum of weighted noncentral chi-square variables, TEST 14 (2) (2005) 397–415, doi:10.1007/BF02595410.

[28] P. Duchesne, P.L.D. Micheaux, Computing the distribution of quadratic forms: further comparisons between the Liu-Tang-Zhang approximation and exact methods, Comput. Stat. Data Anal. 54 (4) (2010) 858–862, doi:10.1016/j.csda.2009.11.025.

[29] J. Sheil, I. O'Muircheartaigh, Algorithm as 106: the distribution of non-negative quadratic forms in normal variables, J. R. Stat. Soc.. Ser. C (Appl. Stat.) 26 (1) (1977) 92–98.

[30] A. Şahin, Y.S. Eroğlu, I. Güvenç, N. Pala, M. Yüksel, Hybrid 3-D localization for visible light communication systems, J. Lightwave Technol. 33 (22) (2015) 4589–4599, doi:10.1109/JLT.2015.2477502.

[31] R. Murray, Z. Li, S. Sastry, A mathmematical introduction to robotic manipulation, 1994.

[32] T. Michel, H. Fourati, P. Genevès, N. Layaïda, A comparative analysis of attitude estimation for pedestrian navigation with smartphones, in: 2015 International Conference on Indoor Positioning and Indoor Navigation (IPIN), 2015, pp. 1–10, doi:10.1109/IPIN.2015.7346767.

[33] H. Fourati, D.E.C. Belkhiat, Multisensor Attitude Estimation: Fundamental Concepts and Applications, CRC Press, 2016.

[34] M. Giurato, M. Lovera, Quadrotor attitude determination: a comparison study, in: 2016 IEEE Conference on Control Applications (CCA), 2016, pp. 21–26, doi:10.1109/CCA.2016.7587816.

[35] G. Troni, L.L. Whitcomb, Experimental evaluation of a MEMS inertial measurements unit for doppler navigation of underwater vehicles, in: 2012 Oceans, 2012, pp. 1–7, doi:10.1109/OCEANS.2012.6405003.

[36] T.Q. Wang, Y.A. Sekercioglu, A. Neild, J. Armstrong, Position accuracy of time-of-arrival based ranging using visible light with application in indoor localization systems, J. Lightwave Technol. 31 (20) (2013) 3302–3308, doi:10.1109/JLT.2013.2281592.

[37] S. Jung, S. Hann, C. Park, TDOA-based optical wireless indoor localization using LED ceiling lamps, IEEE Trans. Consum. Electron. 57 (4) (2011) 1592–1597, doi:10.1109/TCE.2011.6131130.